nature photonics

LETTERS

https://doi.org/10.1038/s41566-022-01019-6

Check for updates

Few-photon all-optical phase rotation in a quantum-well micropillar cavity

Tintu Kuriakose[1], Paul M. Walker[1]✉, Toby Dowling[1], Oleksandr Kyriienko[2], Ivan A. Shelykh[3,4], Phillipe St-Jean[5], Nicola Carlon Zambon[5], Aristide Lemaître[5], Isabelle Sagnes[5], Luc Legratiet[5], Abdelmounaim Harouri[5], Sylvain Ravets[5], Maurice S. Skolnick[1], Alberto Amo[6], Jacqueline Bloch[5] and Dmitry N. Krizhanovskii[1]

Photonic platforms are an excellent setting for quantum technologies as weak photon–environment coupling ensures long coherence times. The second key ingredient for quantum photonics is interactions between photons, which can be provided by optical nonlinearities in the form of cross-phase modulation. This approach underpins many proposed applications in quantum optics[1–7] and information processing[8], but achieving its potential requires strong single-photon-level nonlinear phase shifts as well as scalable nonlinear elements. In this work we show that the required nonlinearity can be provided by exciton–polaritons in micropillars with embedded quantum wells. These combine the strong interactions of excitons[9,10] with the scalability of micrometre-sized emitters[11]. We observe cross-phase modulation of up to 3 ± 1 mrad per polariton using laser beams attenuated to below the average intensity of a single photon. With our work serving as a stepping stone, we lay down a route for quantum information processing in polaritonic lattices.

Quantum applications of cross-phase modulation (XPM) include teleportation[1], photon-number detection[2], metrology[4], cryptography[5] and quantum information processing (QIP), where XPM was proposed as a route to circuit-[6] and measurement-based[7] quantum computing; however, XPM-based photonic QIP faces several challenges. Frequency entanglement can degrade the fidelity[12] of XPM-based quantum gates[3], but this can be overcome by cascading nonlinear resonators, with each providing a moderate phase shift[8]. Such cascading naturally requires scalability of the resonators. The remaining major challenge, which we address in this paper, is to find a system with high enough single-particle XPM phase shift, ϕ_{sp}, which is suitable for scaling.

The small size of atom-like emitters ensures strong interactions and large ϕ_{sp}, but at the same time makes scalability challenging. Real atoms are not easy to trap and manipulate, and it is difficult to achieve many solid-state artificial atoms with deterministic frequencies and locations. Experimentally, ϕ_{sp} from 0.1 to π radians have been observed in atomic ensembles[13–18] and atoms[19] or quantum dots[20,21] strongly coupled to cavities. Methods using electromagnetically induced transparency[16–18] or sequential photon–atom interactions[22,23] achieve $\phi_{sp}=\pi$ using microsecond pulse sequences and milliwatt ancilliary beams, whereas passive nonlinear XPM, as we study here, is favourable for high-rate, low-energy operation. Approaches avoiding atom-like emitters have been hindered by the small optical nonlinearity in typical Kerr media; ϕ_{sp} values from 10^{-4} to 0.3 mrad has been demonstrated with optical fibre[24] and atomic vapours[14,15]. Polariton micropillars, where photons are strongly coupled to excitons[25], are a prime candidate for combining high phase shifts and scalability. Their micrometre dimensions allow scaling into large lattices with deterministic positioning and energies identical within the linewidth[11], whereas the excitonic component of polaritons provides interactions at least 1,000-times larger than in weakly coupled and/or bulk semiconductors[26]. An important feature of polariton interactions is their polarization dependence[27], which can be used to implement all-optical spin switches[28] or break time-reversal symmetry. Polaritonic resonators have been used as a source of weakly sub-Poissonian light[9,10]. However, neither XPM between distinct modes nor the polarization dependence of interactions has been harnessed at the few-particle level.

In this article we demonstrate ϕ_{sp} values of up to 3 mrad, the highest amount without using atom-like emitters. As a proof of principle, we demonstrate this phase rotation using a control laser attenuated down to an average intensity of 0.13 polaritons, where the probability of >1 control polariton being in the system is <1%. We exploit the polarization-dependent interactions to encode the XPM on the polarization state of a second laser, achieving high phase sensitivity and stability. Extrapolating our experimental results to samples with tighter photon confinement and narrower exciton linewidth[9,10], we predict ϕ_{sp} approaching a substantial fraction of π. Using the example of XPM-based conditional-phase (CPHASE) quantum gates, we show theoretically that these experimental results open new routes towards active quantum processing with exciton polaritons.

Our device is an AlGaAs air-post Fabry–Pérot microcavity containing a single quantum well of the type illustrated in Fig. 1a (see Methods and Supplementary Discussion 1). All experiments were performed near liquid helium temperature. We first characterized the micropillar using photoluminescence spectroscopy. The spectrum of discrete states resulting from the three-dimensional optical confinement can be seen in Fig. 1b, with mode intensity profiles shown in Fig. 1.

The phase rotation measurement is illustrated in Fig. 1a (see also Supplementary Discussion 1). We resonantly excited E_{11} with a circularly polarized continuous-wave beam (control beam) and E_{12} with a pulsed beam linearly polarized along the y direction

[1]Department of Physics and Astronomy, University of Sheffield, Sheffield, UK. [2]Department of Physics and Astronomy, University of Exeter, Exeter, UK. [3]Science Institute, University of Iceland, Reykjavik, Iceland. [4]Department of Physics and Technology, ITMO University, St Petersburg, Russia. [5]Centre de Nanosciences et de Nanotechnologies (C2N), Université Paris Saclay—CNRS, Palaiseau, France. [6]Univ. Lille, CNRS, UMR 8523 –PhLAM– Physique des Lasers Atomes et Molécules, Lille, France. ✉e-mail: p.m.walker@sheffield.ac.uk

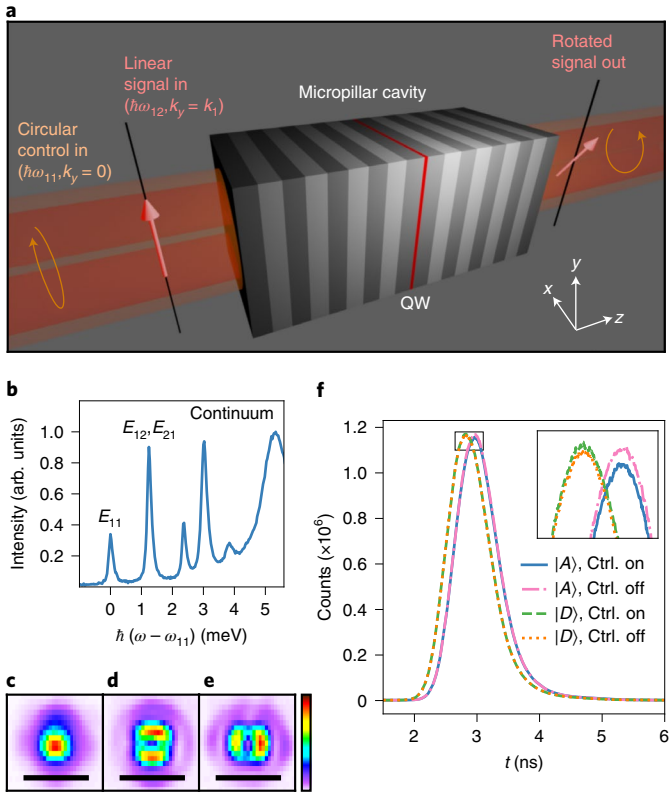

Fig. 1 | Sample properties. a, Schematic of the experimental arrangement. k_y is the y component of the wavevector and k_1 is the non-zero peak wavenumber of the signal state. **b**, Photoluminescence spectrum from pillar A; $\hbar\omega_{11} = 1{,}446$ meV. **c**–**e**, Real space photoluminescence intensity maps taken at the frequencies of the ground (E_{11}) (**c**) and first excited (E_{12} (**d**) and E_{21} (**e**)) manifolds. The scale bar corresponds to 5 μm, which is the size of the micropillar. Colour scale is linear and denotes intensity relative to peak. **f**, Example of raw TCSPC curves recorded during a phase shift measurement; $|D\rangle$ and $|A\rangle$ denote the signals from avalanche photodiodes (APDs) measuring those polarization components while 'Ctrl on' and 'Ctrl off' specify the control beam state. The inset to **f** shows a zoom of the region labelled by a black rectangle.

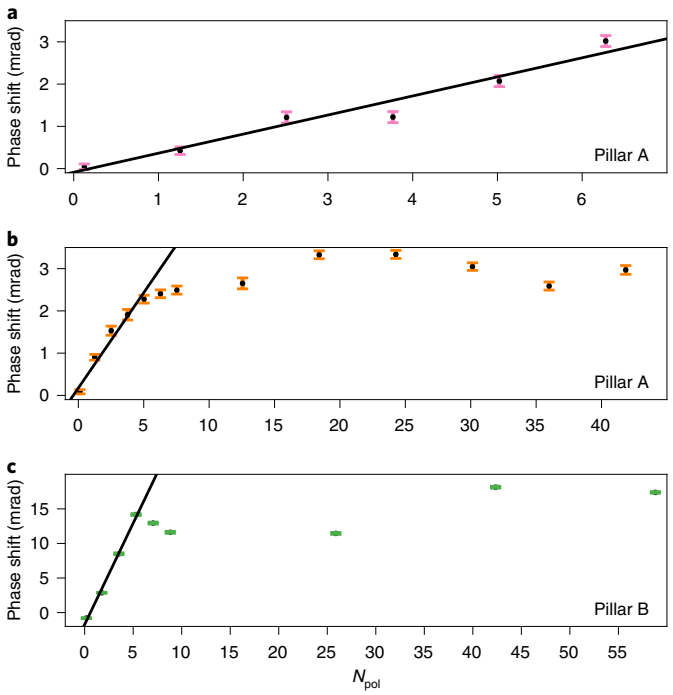

Fig. 2 | Measured phase shift as a function of control beam mean polariton number. a,**b**, Data measured on pillar A on two different days approximately one month apart, with **a** measured before **b**. **c**, Data measured on pillar B. The error bars cover the $\pm 2\sigma$ range, where σ is the s.d. among the repeated measurements of the phase. The solid lines are best fits of straight lines passing through the origin to points, with $N_{pol} < 6$.

(signal beam). The signal linear polarization can be decomposed into two circularly polarized components. As polariton interactions depend strongly on relative circular polarization[27], the presence of the control beam shifts the E_{12} resonance to higher energies only for the polarization parallel to the control beam. Consequently, the co-polarized signal component acquires a relative phase shift via XPM, resulting in a rotation of the signal beam linear polarization angle. Measuring this change in polarization reveals the amount of phase shift. A quantitative analysis of the XPM and detection process is given in Supplementary Discussion 2. The overall nonlinear phase shift ϕ reads

$$\phi = \frac{2(g_1 - g_2)}{\gamma/2}|X_{11}|^2|X_{12}|^2\frac{N_{pol}}{A_{eff}}. \quad (1)$$

Here, N_{pol} is the mean number of control polaritons present in the cavity, A_{eff} is the averaged confinement area of the modes, and γ is the full width at half maximum (FWHM) signal linewidth; g_1 and g_2 are the interaction strengths for co- and cross-circularly-polarized excitons, respectively. The polariton interaction strength increases with the excitonic fractions $|X_{11}|^2$ and $|X_{12}|^2$ of the control and signal states. The nonlinear frequency splitting between circular-polarization states is analogous to a Zeeman splitting caused by an effective magnetic field and the polarization rotation is analogous to the Faraday effect.

To measure the XPM phase shift we collected the transmitted light, filtered out the control beam using a spectrometer, and measured the diagonal ($|D\rangle$) and anti-diagonal ($|A\rangle$) signal polarization components with the control beam alternated between on and off. Intensities were measured using time-correlated single-photon counting (TCSPC), which allowed further separation of the pulsed signal beam from the continuous-wave control (see Methods and Supplementary Discussion 3). An example of the TCSPC data is shown in Fig. 1f. The peaks are due to the signal pulses, whereas effects uncorrelated with the signal pulses form a continuous-wave background, which we measured using points at times far from the peak and subtracted. We then integrated the counts around the peaks to obtain the total signal count rates $I_D^{(on)}$, $I_D^{(off)}$, $I_A^{(on)}$ and $I_A^{(off)}$ for $|D\rangle$ and $|A\rangle$.

The phase shift ϕ is deduced from the difference in polarization degree with the control beam on and off (see Supplementary Discussion 2) and, for small nonlinear resonance shifts compared with the linewidth, is given by

$$\phi \approx \left(\frac{I_D^{(on)} - I_A^{(on)}}{I_D^{(on)} + I_A^{(on)}}\right) - \left(\frac{I_D^{(off)} - I_A^{(off)}}{I_D^{(off)} + I_A^{(off)}}\right). \quad (2)$$

As well as measuring the phase, it is important to accurately deduce N_{pol}. The absolute calibration of which was obtained by measurement of the cavity transfer function, carefully separating the radiative losses from other contributions to the linewidth, which leads to

$$E_{cav} = \hbar\omega N_{pol} = \frac{P_{out}}{\gamma_T|C_{11}|^2} \quad (3)$$

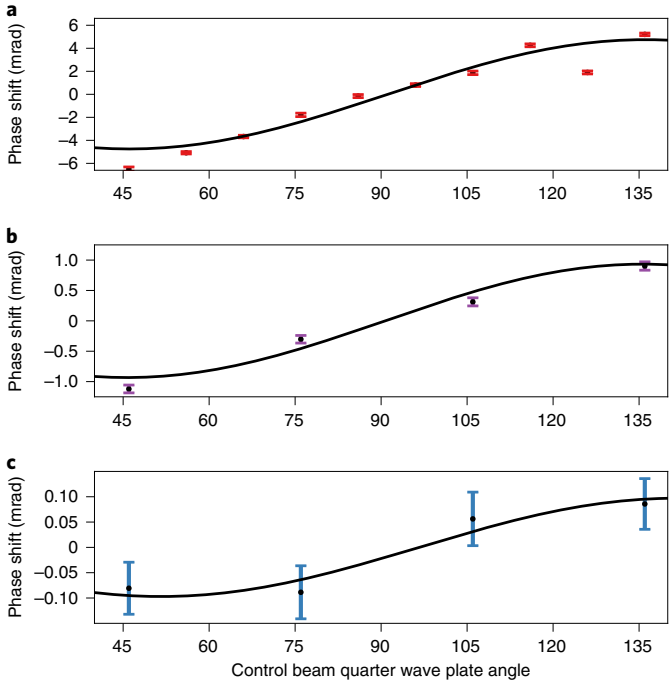

Fig. 3 | Phase shift dependence on control beam polarization. a, $N_{pol} = 42 \pm 8$. **b**, $N_{pol} = 1.3 \pm 0.3$. **c**, $N_{pol} = 0.13 \pm 0.03$. Measurements made on pillar A. Error bars cover the range $\pm 2\sigma$ where σ is the standard deviation among the repeated measurements of the phase. Solid black lines are best-fit sinusoids.

(see Methods, and Supplementary Discussion 4 and 5). Here P_{out} is the transmitted power and γ_T is the portion of the bare cavity linewidth associated with transmission through the mirror towards the detector; $|C_{11}|^2 = 1 - |X_{11}|^2$ is the control polariton photonic fraction. We confirmed the accuracy of equation (3) by exactly solving Maxwell's equations for a wide range of cavity parameters around those of the experimental device (see Supplementary Discussion 5).

The phase change versus N_{pol} is plotted in Fig. 2. We considered two different micropillar cavities (A and B) with different exciton fractions and linewidths (see Methods). The phase shift increases with increasing N_{pol} between 0.1 and 6 polaritons. Fitting straight lines in this region we deduce slopes of 0.5 ± 0.2 and 0.5 ± 0.3 mrad per polariton for the two pillar A datasets (Fig. 2a,b). For pillar B, which has 7.2-times larger $|X_{11}|^2|X_{12}|^2$ (see Methods), the slope was 3 ± 1 mrad per polariton.

At above ~6 polaritons (Fig. 2b,c), the phase shift saturates for both pillars. Further experiments are needed to identify the mechanism behind this saturation. The dependence on control polarization is preserved even up to 42 polaritons (Fig. 3a), but with reduced magnitude, which suggests that saturation is due to suppression of the polarization dependence of the effective polariton nonlinearity, or of the control polariton circular polarization degree. These can occur due to interaction with a reservoir of excitons, which can be enhanced by sample heating[29–31]. Reservoir accumulation and thermal effects can be overcome using pulsed rather than continuous-wave control excitation[26,30], and by reducing the density of reservoir states using samples with smaller exciton inhomogeneous broadening[32]. We note that saturation will not be detrimental to performance as devices will operate with $N_{pol} \leq 1$.

Upon inserting our measured slopes for $\phi(N_{pol})$ into equation (1), we find they are consistent with $g_1 - g_2 = 11 \pm 4\,\mu eV\,\mu m^2$ and $10 \pm 4\,\mu eV\,\mu m^2$ for pillars A and B, respectively. These are at the lower end of the range established by many groups[9,10,26,33–36], indicating that we do not underestimate N_{pol}. The agreement between pillars shows that the phase shift scales with exciton fraction as expected. The value of 3 mrad per polariton in pillar B is consistent with a blue-shift of only 0.062 μeV per polariton compared to the E_{12} state linewidth 83 μeV, which highlights the sensitivity of the technique.

Table 1 | Comparison of XPM phase shift platforms

System	ϕ per particle (mrad)
Rydberg atoms in EIT regime[17]	3,300
Single caesium atom[13]	280
Strongly coupled quantum dot[20]	220
This work	3 ± 1
Rubidium vapour in a hollow-core fibre[14]	0.3
Metastable xenon[15]	0.0003
Photonic crystal fibre[24]	0.0001

For our proposed Faraday-like phase rotation mechanism the induced phase should follow a sinusoidal dependence on the angle of the quarter-wave plate used to set the control polarization, vanishing when the control is linearly polarized and reversing sign when it is switched to the opposite circular polarization (see Supplementary Discussion 2). In Fig. 3 we show the phase shift versus the quarter-wave plate angle for three different control beam strengths covering two orders of magnitude. It agrees well with the theoretical prediction for all control powers, reducing to zero at around 90° and then reversing sign. We note that the absolute magnitude of the phase shifts is different to those in Fig. 2 due to day-to-day drifts in sensitivity (see Methods).

Finally, we discuss the measurements of phase at very low N_{pol} of 0.13 ± 0.03. The data in Fig. 2a and Fig. 2b give phase shifts of 0.04 ± 0.06 and 0.08 ± 0.05 mrad, respectively. The four points in Fig. 3c produce phase shifts larger than the uncertainty given by the error bars. We are thus able to measure a phase shift for average powers $N_{pol} = 0.13$, where the probability of the pillar being occupied by a single photon is 11% and the probability of an occupancy greater than 1 is less than 0.8%, based on the Poissonian statistics expected for laser fields. We are thus well inside the single-photon regime.

In Table 1 we compare the phase shifts of various systems. Our phase shift of 3 mrad per particle is one order of magnitude larger than in the nearest competing system, which does not use atom-like emitters with their associated scalability challenges (see Supplementary Discussion 6 for a more detailed comparison). We predict that in samples with tighter photon confinement and narrower exciton linewidth[9], the phase shift could be two orders of magnitude larger (see Supplementary Discussion 7). Moreover, an additional approximately tenfold increase in interactions can also be obtained using dipolar polaritons[37] or trion polaritons[38].

We measure control (signal) beam transmissions of 45% (35%) in our current devices, limited by a combination of imperfect mode-matching and absorptive losses (see Supplementary Discussion 8 for more details). Transmission can realistically be increased above 90% using lower temperature ~4 K and GaAs quantum wells, which have lower inhomogeneous broadening[32]. This would allow transmission through multiple pillars with a $1/e$ decay of approximately ten sites. The signal transmission is independent of control polarization and has a weak dependence on control power arising from blue-shift of the states relative to resonance with the signal laser (Methods). To maximize transmission, low sample temperatures of 4 K (easily achieved using commercial closed-cycle cryostats) are important, in comparison to refs. [14,15,18,24], where room temperature phase shifts were demonstrated.

Having demonstrated XPM for single-polariton intensities it is interesting to consider whether XPM-based effects can be used for polaritonic QIP. Entanglement between frequency states was shown to limit the fidelity of XPM-based CPHASE gates for large phase shifts[12]. This obstacle can be overcome if nonlinearity is distributed over several cavities with cascaded wavepacket propagation[8]. In Supplementary Discussion 9 we analyse theoretically a potential scheme to achieve this. It requires scattering through order ten resonators and optical circulation (suppressed backscattering). Micropillar lattices of this scale are regularly produced, whereas directional propagation from one phase-shift element to the next can be achieved using the edge states in polariton topological insulator lattices and benefit from the rich topological physics of polaritons[39].

As we show in Supplementary Fig. 10, CPHASE gate fidelity depends on the size of the single-pillar phase shifts and the target phase. Full π shift, corresponding to high-fidelity controlled-Z gate, requires large single-pillar nonlinearity-to-linewidth ratio U_{pp}/γ; however, near-perfect-fidelity π/m gates (where m is an integer) can even be achieved at $U_{pp}/\gamma < 1$. When concatenated, these contribute to a universal gateset and, at $m = 6$, have been used in quantum hardware-based solution of optimization problems[40].

Although a distant goal, we consider the ability to inject nonlinearity at the single polariton level a crucial element for many QIP protocols. In general terms, our quantum well polariton approach to single photon phase shifts provides the tools to optimize the balance between scalability and interaction strength for any given application. In summary, we demonstrated a few-particle polariton XPM phase shift in a scalable on-chip platform. This opens up new approaches to a wide class of nonlinear quantum optical phenomena, and offers a route towards QIP with polaritonic lattices.

Online content

Any methods, additional references, Nature Research reporting summaries, source data, extended data, supplementary information, acknowledgements, peer review information; details of author contributions and competing interests; and statements of data and code availability are available at https://doi.org/10.1038/s41566-022-01019-6.

Received: 8 June 2021; Accepted: 9 May 2022;
Published online: 16 June 2022

References

1. Vitali, D., Fortunato, M. & Tombesi, P. Complete quantum teleportation with a kerr nonlinearity. *Phys. Rev. Lett.* **85**, 445–448 (2000).
2. Munro, W. J., Nemoto, K., Beausoleil, R. G. & Spiller, T. P. High-efficiency quantum-nondemolition single-photon-number-resolving detector. *Phys. Rev. A* **71**, 033819 (2005).
3. Spiller, T. P. et al. Quantum computation by communication. *New J. Phys.* **8**, 30–30 (2006).
4. Joo, J., Munro, W. J. & Spiller, T. P. Quantum metrology with entangled coherent states. *Phys. Rev. Lett.* **107**, 083601 (2011).
5. Simon, D. S., Jaeger, G. & Sergienko, A. V. Entangled-coherent-state quantum key distribution with entanglement witnessing. *Phys. Rev. A* **89**, 012315 (2014).
6. Chuang, I. L. & Yamamoto, Y. Simple quantum computer. *Phys. Rev. A* **52**, 3489–3496 (1995).
7. Hutchinson, G. D. & Milburn, G. J. Nonlinear quantum optical computing via measurement. *J. Modern Optics* **51**, 1211–1222 (2004).
8. Brod, D. J., Combes, J. & Gea-Banacloche, J. Two photons co- and counterpropagating through N cross-Kerr sites. *Phys. Rev. A* **94**, 023833 (2016).
9. Delteil, A. et al. Towards polariton blockade of confined exciton–polaritons. *Nat. Mate.* **18**, 219–222 (2019).
10. Muñoz-Matutano, G. et al. Emergence of quantum correlations from interacting fibre-cavity polaritons. *Nat. Mater.* **18**, 213–218 (2019).
11. Amo, A. & Bloch, J. Exciton-polaritons in lattices: a non-linear photonic simulator. *C. R Phys.* **17**, 934–945 (2016).
12. Shapiro, J. H. Single-photon Kerr nonlinearities do not help quantum computation. *Phys. Rev. A* **73**, 062305 (2006).
13. Turchette, Q. A., Hood, C. J., Lange, W., Mabuchi, H. & Kimble, H. J. Measurement of conditional phase shifts for quantum logic. *Phys. Rev. Lett.* **75**, 4710–4713 (1995).
14. Venkataraman, V., Saha, K. & Gaeta, A. L. Phase modulation at the few-photon level for weak-nonlinearity-based quantum computing. *Nat. Photon.* **7**, 138–141 (2012).
15. Hickman, G. T., Pittman, T. B. & Franson, J. D. Low-power cross-phase modulation in a metastable xenon-filled cavity for quantum-information applications. *Phys. Rev. A* **92**, 053808 (2015).
16. Liu, Z.-Y. et al. Large cross-phase modulations at the few-photon level. *Phys. Rev. Lett.* **117**, 203601 (2016).
17. Tiarks, D., Schmidt, S., Rempe, G. & Dürr, S. Optical π phase shift created with a single-photon pulse. *Sci. Adv.* **2**, e1600036 (2016).
18. Sagona-Stophel, S., Shahrokhshahi, R., Jordaan, B., Namazi, M. & Figueroa, E. Conditional π-phase shift of single-photon-level pulses at room temperature. *Phys. Rev. Lett.* **125**, 243601 (2020).
19. Volz, J., Scheucher, M., Junge, C. & Rauschenbeutel, A. Nonlinear π phase shift for single fibre-guided photons interacting with a single resonator-enhanced atom. *Nat. Photon.* **8**, 965–970 (2014).
20. Fushman, I. et al. Controlled phase shifts with a single quantum dot. *Science* **320**, 769–772 (2008).
21. Englund, D. et al. Ultrafast photon-photon interaction in a strongly coupled quantum dot-cavity system. *Phys. Rev. Lett.* **108**, 093604 (2012).
22. Hacker, B., Welte, S., Rempe, G. & Ritter, S. A photon–photon quantum gate based on a single atom in an optical resonator. *Nature* **536**, 193–196 (2016).
23. Sun, S., Kim, H., Luo, Z., Solomon, G. S. & Waks, E. A single-photon switch and transistor enabled by a solid-state quantum memory. *Science* **361**, 57–60 (2018).
24. Matsuda, N., Shimizu, R., Mitsumori, Y., Kosaka, H. & Edamatsu, K. Observation of optical-fibre kerr nonlinearity at the single-photon level. *Nat. Photon.* **3**, 95–98 (2009).
25. Bajoni, D. et al. Polariton laser using single micropillar GaAs-GaAlAs semiconductor cavities. *Phys. Rev. Lett.* **100**, 047401 (2008).
26. Walker, P. M. et al. Dark solitons in high velocity waveguide polariton fluids. *Phys. Rev. Lett.* **119**, 097403 (2017).
27. Vladimirova, M. et al. Polariton-polariton interaction constants in microcavities. *Phys. Rev. B* **82**, 075301 (2010).
28. Amo, A. et al. Exciton–polariton spin switches. *Nat. Photon.* **4**, 361–366 (2010).
29. Vishnevsky, D. V., Solnyshkov, D. D., Gippius, N. A. & Malpuech, G. Multistability of cavity exciton polaritons affected by the thermally generated exciton reservoir. *Phys. Rev. B* **85**, 155328 (2012).
30. Sekretenko, A. V., Gavrilov, S. S. & Kulakovskii, V. D. Polariton-polariton interactions in microcavities under a resonant 10 to 100 picosecond pulse excitation. *Phys. Rev. B* **88**, 195302 (2013).
31. Ouellet-Plamondon, C. et al. Reservoir-induced decoherence of resonantly excited confined polaritons. *Phys. Rev. B* **95**, 085302 (2017).
32. Borri, P., Langbein, W., Woggon, U., Jensen, J. R. & Hvam, J. M. Microcavity polariton linewidths in the weak-disorder regime. *Phys. Rev. B* **63**, 035307 (2000).
33. Amo, A. et al. Superfluidity of polaritons in semiconductor microcavities. *Nat. Phys.* **5**, 805–810 (2009).
34. Vladimirova, M. et al. Polarization controlled nonlinear transmission of light through semiconductor microcavities. *Phys. Rev. B* **79**, 115325 (2009).
35. Brichkin, A. S. et al. Effect of Coulomb interaction on exciton-polariton condensates in GaAs pillar microcavities. *Phys. Rev. B* **84**, 195301 (2011).
36. Estrecho, E. et al. Direct measurement of polariton-polariton interaction strength in the thomas-fermi regime of exciton-polariton condensation. *Phys. Rev. B* **100**, 035306 (2019).
37. Rosenberg, I. et al. Strongly interacting dipolar-polaritons. *Sci. Adv.* **4**, eaat8880 (2018).
38. Emmanuele, R. P. A. et al. Highly nonlinear trion-polaritons in a monolayer semiconductor. *Nat. Commun.* **11**, 3589 (2020).
39. Solnyshkov, D. D. et al. Microcavity polaritons for topological photonics [invited]. *Opt. Mater. Express* **11**, 1119 (2021).
40. Harrigan, M. P. et al. Quantum approximate optimization of non-planar graph problems on a planar superconducting processor. *Nat. Phys.* **17**, 332 (2021).

Methods

Sample properties. The sample consists of a GaAs cavity containing a single 15-nm-wide $In_{0.05}Ga_{0.95}As$ quantum well at the electric field antinode and embedded between two $Al_{0.1}Ga_{0.9}As/Al_{0.95}Ga_{0.05}As$ Bragg mirrors. Confinement of the light in all three dimensions results in discrete optical modes, which were measured using imaging photoluminescence spectroscopy (Fig. 1b–e). The transverse mode profiles are similar to Hermite–Gauss modes. In the ground state manifold, labelled E_{11}, there are two degenerate polarization states. In the first excited manifold the sub-manifolds E_{12} and E_{21}, have non-zero wavevector component in the y and x direction respectively and each contains two orthogonal polarization states. There is a small splitting among these four states due to a combination of TE–TM splitting and the pillars not being perfectly square. The splitting between the E_{21} and E_{12} submanifolds allowed them to be mapped separately (Fig. 1d,e) using energies one FWHM either side of the peak (see Methods).

The studied sample contains many pillars with different sizes (2–5 μm width) to allow tuning of the spatial distribution of modes and their energy separation. The spacing between individual pillars was 10 μm. Different detunings of pillar modes with respect to the quantum-well exciton resonance were also available due to a wedge in the molecular-beam-epitaxy-grown cavity. The experiments presented in this paper were performed on 5 μm × 5 μm square pillars. The square geometry allowed simple excitation of the Hermite–Gauss-like first excited state compared to more difficult beam shaping required to excite the Laguerre–Gauss-like excited states of a circular pillar. The 5 μm size of the pillars minimized TE–TM splitting of the first excited manifold.

The sample Rabi splitting 3.4 ± 0.1 meV was obtained from a coupled exciton-photon oscillator model fit to the dispersion of pillar modes. To determine the detuning of the modes from the exciton we compared the energy splitting between the E_{11} and E_{12} modes with the value for very negatively detuned pillars. The splitting reduces as the photonic fraction reduces and so can be used to directly obtain the photonic (and hence excitonic) fraction of the polaritons. For pillar A the exciton fractions in the control and signal modes were $|X_{11}|^2 \approx 9\%$ and $|X_{12}|^2 \approx 15\%$, respectively. For pillar B they were $|X_{11}|^2 \approx 25\%$ and $|X_{12}|^2 \approx 42\%$.

The polariton linewidths (90 μeV and 83 μeV for pillars A and B, respectively) were measured by monitoring the transmitted intensity of a single mode laser as it was scanned through the modes. The measured linewidths are considerably larger than the planar cavity linewidths predicted by transfer matrix method (20–30 μeV), which is most likely due to absorptive losses associated with elevated sample temperature. In the type of sample-in-vacuum, cold-finger cryostats that we used, sample temperatures were typically higher (~10–20 K) than the 4 K temperature measured at the heat-exchanger, owing to radiation through cryostat optical windows and limited thermal conductivity between the sample and the liquid helium loop. In other types of cryostat (for example, the sample-in-vapour type), lower temperatures of ~4 K can be achieved. We note that for deducing the number of polaritons we use the fraction of the linewidth due to radiative transmission towards the detector, $\gamma_T = 14 \pm 3$ μeV in equation (3) (see Methods). This was calibrated at detunings far from the exciton, where absorption is negligible.

The effective mode area for nonlinear interactions A_{eff} is defined in Supplementary Discussion 2 following the standard formula from nonlinear fibre optics. It has the same value $A_{eff} = 17$ μm² for both pillars. It was calculated using the modes of a square dielectric rod of GaAs in air obtained from the commercial eigenmode solver Lumerical MODE.

Common experimental details. Experiments were performed near to liquid helium temperature. The sample was held in vacuum and mounted to a copper block connected to the heat-exchanger of a continuous flow cryostat. The copper block was held at less than 5 K, as measured using a silicon diode temperature sensor. The radiation load through the cryostat windows and the small transverse area for heat flow in a 5 μm size micropillar may have caused the actual pillar temperatures to be higher.

The micropillars were optically excited directly (not through the substrate) using a 4 mm focal length objective (numerical aperture 0.42). Light emitted by or transmitted through the pillars was collected by a 10 mm focal length microscope objective (numerical aperture 0.6) and imaged via a set of confocal lenses onto the entrance slit of an imaging spectrometer. The spectrometer output could be switched between a CCD camera and an exit slit used to select only the signal beam for the APD measurements. The spectrometer exit slit was imaged onto the APDs via another pair of confocal lenses.

Photoluminescence experiments. For the non-resonant photoluminescence experiments excitation was with a laser at ~830 nm, above the quantum well band edge, and all optical states were then populated by hot carrier relaxation. The photoluminescence spectra were recorded using a CCD camera. Mode intensity profiles were obtained by scanning the images of the modes across the spectrometer entrance slit. E_{12} and E_{21} were mapped separately using frequencies at one FWHM (70–90 μeV) either side of the peak. This relies on a small energy splitting between E_{12} and E_{21} most likely caused by slightly non-square pillars. As can be seen in Fig. 1b, the splitting was too small to resolve directly from the spectrum.

Phase rotation measurement details. For the phase rotation experiments, we resonantly excited the micropillar ground state with a circularly polarized control beam emitted by a continuous-wave single-mode laser. At the same time, we also excited the E_{12} pillar mode with a linearly polarized signal beam from a tuneable mode-locked titanium:sapphire laser with a pulse duration of ~100 ps and a repetition rate of 80 MHz. The sizes and divergences of the input control and signal beams were controlled with telescopes to match those of the pillar modes and hence optimally couple light to the microcavity. Both the signal and control beam were set to have a flat-phase beam waist of ~3 μm (FWHM) on the sample surface, matching the ground-mode FWHM. After this, a phase mask was placed at the focus of the telescope controlling the signal beam to introduce a π phase jump at the centre of the signal spot on the sample surface. In this way, the signal beam was converted to a Hermite–Gauss-like beam with symmetry matching that of the E_{12} mode but of the wrong symmetry to excite the E_{21} mode. To ensure that experimental drifts did not compromise optimal coupling the transmission of the control and signal beams was checked after every data point shown in Figs. 2 and 3 and reoptimized if necessary.

Measurement of the intensities of the two polarization components was performed by photon counting using APDs owing to their extremely small noise level. The control beam was chopped on and off at a rate of 10 kHz using an electro-optic modulator driven by a square wave control signal. Counts from the APDs were sent to a TCSPC card via a router that encoded information about which APD detected the photon, and whether the chopped control beam was on or off. The signal beam was attenuated so that on average 0.025 photons were detected per laser pulse. We avoided spurious signals in several ways. As the control beam was a continuous wave whereas the signal was pulsed (see Fig. 1f), we were able to remove any potential scattered control light reaching the APDs by subtracting the continuous wave background from the data. This also removed any dark or APD after-pulsing counts. The true signal counts were then obtained by summing counts around the signal peaks in the TCSPC traces. As we measure a polarization degree of the form shown in equation (2) any overall drifts or jitter in signal beam intensity or integration time simply cancel out. Our chopping of the control beam at 10 kHz eliminates any control drift effects in a manner similar to lock-in detection, while collection over several minutes effectively averages out control beam jitter. Further details are given in Supplementary Discussion 3.

Number of polaritons. The number of control polaritons in the pillar N_{pol} was deduced using the transmitted power and the radiative loss rate through the mirror on the transmission side of the sample, γ_T. The accuracy of equation (3) was confirmed by comparison of transmitted power and stored electromagnetic energy using exact solutions of Maxwell's equations (transfer matrix method) for cavities with a wide range of parameters around those of the experimental device (see Supplementary Discussion 5 for a detailed discussion).

The total radiative loss through both mirrors was obtained by measuring the linewidth $\gamma_{DBR} = 25 \pm 5$ μeV at a very photonic detuning where the losses are dominated by the finite reflectivity of the mirrors. It agrees well with transfer matrix simulations. We then use $\gamma_T = \eta\gamma_{DBR}$ where $\eta = 0.553$ is related to the relative mirror strengths and was obtained from the transfer matrix simulations.

In principle either the incident or transmitted power can be used to obtain N_{pol}. We obtain a high transmission through the pillar with transmitted/incident power being 40% (45%) for the control state of pillar A (B). It is more accurate to use the transmitted power since incident power can be reflected due to imperfect mode matching.

The signal state transmission was 35% for the best coupling to the pillars that we achieved. The laser pulses incident on the pillar contained 27 photons on average. The transmitted pulses contained between 3 and 9 photons depending on coupling, corresponding to peak internal number of polaritons between 2 and 5 for pillar A, and 3 and 8 for pillar B. We did not observe any dependence of the results on the number of signal polaritons.

The dependence of total signal beam transmission on the control was obtained by adding the intensities of both APDs (See Supplementary Discussion 8). We found no systematic dependence of the signal transmission on control beam polarization. The signal transmission versus control power varied with gradient similar in magnitude to the phase shift and with either positive or negative sign depending on the dataset. This is consistent with a blue-shift of the states shifting them further into or out of resonance with the signal laser (see Supplementary Discussion 2).

Statistical analysis. By calculating the mean and standard deviation σ among many (10^3–10^4) repeated measurements of ϕ, we directly obtain the average phase change and its uncertainty for each value of N_{pol} or quarter wave plate angle. The quoted uncertainties are $\pm 2\sigma$ and the error bars are plotted covering the range from -2σ to $+2\sigma$, which corresponds to the 95% confidence interval for a normal distribution.

Sources of noise in the data. There are two categories of noise contributing to the data shown in Figs. 2 and 3. These are a random error in the phase of each individual data point, and systematic variations in sensitivity which occurred between individual data points and different data sets (see Supplementary

Discussion 3). The former arises from the Poissonian counting statistics. The latter arises because sub-linewidth changes in signal beam detuning can change the sensitivity of the measurement to the blue-shift of the states. The small changes in detuning were caused by slow frequency drift during data collection, necessitating slight retuning between data points, and also by the coarse tuning (limited to ~20–30 μeV accuracy) of our 100 ps pulsed laser. The sensitivity function is Lorentzian with the state linewidth (see Supplementary Discussion 2). During data collection, small experimental drifts were corrected in between recording each data point, resulting in small changes in sensitivity and hence some point-to-point noise. Nevertheless, the overall trends are clearly visible in the curves presented in Figs. 2 and 3 and they agree well with theory so we can be confident that this point-to-point noise is not too large. The dependence of sensitivity on small changes in signal laser detuning also causes small differences in scaling from one data set to another, hence the best-fit peak phase shift for $N_{pol}=42$ polaritons in Fig. 3a is 5 ± 1 mrad, which is slightly larger than the maximum value in Fig. 2b (3.3 ± 0.1), which was measured on a different day.

Data availability

The data supporting the findings of this study are freely available in the University of Sheffield repository with the identifier https://doi.org/10.15131/shef.data.14744121.

Code availability

The custom codes used in this study are available from the corresponding author on reasonable request.

Acknowledgements

This work was supported by the Engineering and Physical Sciences Research Council grants EP/N031776/1 and EP/V026496/1, the QUANTERA project Interpol (EP/R04385X/1 and ANR-QUAN-0003-05), the Paris Ile-de-France Région in the framework of DIM SIRTEQ, ERC StG ARQADIA (949730) and CoG EMERGENTOPO (865151), the Marie Skłodowska-Curie individual fellowship ToPol, the H2020-FETFLAG project PhoQus (820392) and the French RENATECH network. O.K. acknowledges the support from UK EPSRC New Investigator Award (EP/V00171X/1). A.A. acknowledges support from the Labex CEMPI (ANR-11-LABX-0007). I.A.S. acknowledges support from IRF (project 'Hybrid polaritonics') and Priority 2030 Federal Academic Leadership Program.

Author contributions

P.M.W. and D.N.K. conceived and designed the experiment. T.K., P.M.W. and T.D. built the experimental apparatus and performed the experiments. P.S-J, N.C.Z., A.A., S.R. and J.B. designed and characterized the sample. A.L, IS, L.L and A.H fabricated the sample. P.M.W. analysed the data, and wrote the manuscript and Supplementary Information with contributions from T.K. and O.K. O K. developed the quantum theoretical description of XPM CPHASE gates. P.M.W. developed the classical theory for cavity occupancy and XPM polariton polarization rotation. All authors contributed to discussion of the data, and discussion and revision of the manuscript.

Competing interests

The authors declare no competing interests.

Additional information

Supplementary information The online version contains supplementary material available at https://doi.org/10.1038/s41566-022-01019-6.

Correspondence and requests for materials should be addressed to Paul M. Walker.

Peer review information *Nature Photonics* thanks Fetah Benabid and the other, anonymous, reviewer(s) for their contribution to the peer review of this work.

Reprints and permissions information is available at www.nature.com/reprints.